Engineering Optimization

ISSN: 0305-215X (Print) 1029-0273 (Online) Journal homepage: http://www.tandfonline.com/loi/geno20

Topology optimization of geometrically nonlinear structures using an evolutionary optimization method

Meisam Abdi, Ian Ashcroft & Ricky Wildman

To cite this article: Meisam Abdi, Ian Ashcroft & Ricky Wildman (2018): Topology optimization of geometrically nonlinear structures using an evolutionary optimization method, Engineering Optimization, DOI: 10.1080/0305215X.2017.1418864

To link to this article: https://doi.org/10.1080/0305215X.2017.1418864

Published online: 19 Jan 2018.

ENGINEERING OPTIMIZATION, 2018
https://doi.org/10.1080/0305215X.2017.1418864

Taylor & Francis
Taylor & Francis Group

Topology optimization of geometrically nonlinear structures using an evolutionary optimization method

Meisam Abdi [a,b], Ian Ashcroft [a] and Ricky Wildman [a]

[a]Faculty of Engineering, University of Nottingham, Nottingham, UK; [b]Faculty of Technology, De Montfort University, Leicester, UK

ABSTRACT

The topology optimization using isolines/isosurfaces and extended finite element method (Iso-XFEM) is an evolutionary optimization method developed in previous studies to enable the generation of high-resolution topology optimized designs suitable for additive manufacture. Conventional approaches for topology optimization require additional post-processing after optimization to generate a manufacturable topology with clearly defined smooth boundaries. Iso-XFEM aims to eliminate this time-consuming post-processing stage by defining the boundaries using isovalues of a structural performance criterion and an extended finite element method (XFEM) scheme. In this article, the Iso-XFEM method is further developed to enable the topology optimization of geometrically nonlinear structures undergoing large deformations. This is achieved by implementing a total Lagrangian finite element formulation and defining a structural performance criterion appropriate for the objective function of the optimization problem. The Iso-XFEM solutions for geometrically nonlinear test cases implementing linear and nonlinear modelling are compared, and the suitability of nonlinear modelling for the topology optimization of geometrically nonlinear structures is investigated.

ARTICLE HISTORY
Received 25 October 2016
Accepted 22 November 2017

KEYWORDS
Topology optimization; XFEM; geometrically nonlinear; evolutionary; mesh refinement

1. Introduction

There has been significant interest in topology optimization methods and applications over the past three decades, stemming from the groundbreaking article of Bendsøe and Kikuchi (1988), which introduced the homogenization method. Other methods developed after this include solid isotropic material with penalization (SIMP) (Bendsøe 1989; Zhou and Rozvany 1991), evolutionary structural optimization (ESO) (Xie and Steven 1993; Xie and Steven 1997), bidirectional evolutionary structural optimization (BESO) (Querin, Steven, and Xie 1998; Yang *et al.* 1999; Aremu *et al.* 2013), level-set method (Wang, Wang, and Guo 2003; Allaire, Jouve, and Toader 2004) and evolutionary-based algorithms, *e.g.* the genetic algorithm (GA) (Jakiela *et al.* 2000) and differential evolution (DE) (Fiore *et al.* 2016). Although many of the proposed topology optimization algorithms have been demonstrated for classical problems, such as Michell-type structures and cantilever beams with rectangular domains, less attention has been paid to applying these algorithms to three-dimensional (3D), real-life structures and real loading scenarios. In some cases, the mathematical complexity or the size of the finite element (FE) design domain does not allow the algorithm to be properly implemented. OptiStruct

CONTACT Meisam Abdi meisam.abdi@dmu.ac.uk

(Altair Engineering) is an example of software designed to enable the SIMP method of topology optimization to be applied to real components. Other software such as Nastran (MSC Software) and Abaqus FEA (Dassault Systèmes) also have options to apply similar density-based approaches to find the solution to topology optimization problems. Although the topology optimization modules of these software applications are widely used for research and engineering purposes, a drawback of the density-based approaches (and many other element-based approaches) is that they cannot provide a clear and smooth representation of the design boundaries in converged topologies. This issue brings difficulties in interpreting the solutions, combining them with computed-aided design and manufacturing the topologies. Therefore, the solutions usually need post-processing, reanalysing and shape optimization before manufacturing.

Previous attempts to improve the surface quality of optimized solutions include the use of remeshing/adaptive mesh techniques with topology optimization. Aremu *et al.* (2011) presented a hybrid algorithm for topology optimization consisting of a modified form of the BESO method and an adaptive meshing strategy. A level-set-based r-refinement method was proposed by Yamasaki, Yamanaka, and Fujita (2017) to generate a conforming mesh during the topology optimization process. The use of hierarchical remeshing strategies for the BESO method was investigated by Panesar *et al.* (2017). Nana, Cuillière, and Francois (2016) employed h-refinement to improve definition of the solid–void interface of SIMP solutions. Wang, Kang, and He (2013, 2014) proposed an adaptive mesh refinement strategy based on independent point-wise density interpolation for topology optimization. The idea was to refine the displacement field and the density field separately, aiming to achieve solutions with high quality at a reasonable computational cost. As an alternative to adaptive topology optimization, the topology optimization using isolines/isosurfaces and extended finite element method (Iso-XFEM) was developed in a previous study to address the issues related to the boundary representation of the topology (Abdi, Wildman, and Ashcroft 2014; Abdi, Ashcroft, and Wildman 2014, 2014). The idea was to use a simple evolutionary-based optimization algorithm (similar to BESO) while improving the boundary representation by implementing an isoline/isosurface approach during the optimization. An extended finite element method (XFEM) integration scheme was also used to increase the accuracy of FE solutions near the design boundary. The method was successfully applied to two-dimensional (2D) and 3D structures with complex design domains (Abdi, Ashcroft, and Wildman 2014), and the results showed a significant improvement in boundary representation and structural performance of the solutions over conventional BESO.

The majority of work regarding topology optimization of structures is based on linear modelling of the problems, assuming that the structure contains only linear elastic materials and undergoes small displacements. Although this assumption can be effectively applied to a large range of structural design problems, there are still many cases that require nonlinear modelling to obtain valid solutions. Large deformation is a significant source of nonlinearity that can be found in many nonlinear problems. Examples of such problems include energy absorption structures and compliant mechanisms, which can be classified generally as 'geometrically nonlinear structures'.

A number of previous works considered geometric nonlinearity in topology optimization problems. Jog (1996) used a perimeter method for topology design problems of nonlinear thermoelasticity. Bruns and Tortorelli (1998) introduced a Gaussian weighted density measure for solving topology optimization problems of geometrically nonlinear structures and compliant mechanisms. The examples provided in the above-mentioned studies were not able to show clearly a significant difference in the converged topologies or values of the objective function between linear and nonlinear modelling (Buhl, Pedersen, and Sigmund 2000). Buhl, Pedersen, and Sigmund (2000) coupled SIMP with a nonlinear FE formulation to address the topology optimization of geometrically nonlinear problems. With the examples provided, Buhl and colleaugues showed that in many cases, the solutions from the nonlinear modelling are only slightly different from the linear ones. However, if snap-through effects are involved in the problems, the difference could be significant. Gea and Luo (2001) proposed a microstructure-based design approach with a nonlinear FE formulation for the topology optimization of structures with geometric nonlinearity. Pedersen, Buhl, and Sigmund (2001)

considered topology optimization of nonlinear compliant mechanisms represented with frame elements. Bruns and Tortorelli (2003) proposed an element removal and reintroduction strategy for topology optimization problems with geometric nonlinearity. Ha and Cho (2008) and Luo and Tong (2008) developed a level-set-based topology optimization method for large-deformation problems. Huang and Xie (2007, 2008) applied BESO for topology optimization of geometrically nonlinear structures under both force loading and displacement loading.

An important consideration when applying topology optimization techniques to nonlinear structures should be the computational efficiency of the method, as the analysis requires much more computation than that of a linear structure. This becomes even more important when applying the method to 3D structures. The other issue that may arise in density-based topology optimization approaches such as SIMP is the existence of intermediate densities in the solutions. Because of the large displacements, the tangent stiffness matrix of low-density elements may become indefinite or even negatively definite during the optimization process (Buhl, Pedersen, and Sigmund 2000; Bruns and Tortorelli 2003). To overcome this issue, Bruns and Tortorelli (2003) proposed totally removing low-density elements. To stabilize the excessive distortion of low-density elements, Lahuerta *et al.* (2013) proposed the use of a polyconvex constitutive model in conjunction with a relaxation function. Wang *et al.* (2014) proposed a new interpolation scheme in which the strain energy density (SED) of low-density elements and high-density elements was modelled using small deformation theory and large deformation theory, respectively. An element deformation scaling approach was used by van Dijk, Langelaar, and van Keulen (2014) to scale the local internal displacements in low-density elements. Huang and Xie (2007, 2008) suggested using hard-kill BESO to increase the computational efficiency and avoid issues regarding the existence of intermediate-density elements.

The application of the Iso-XFEM method to the topology optimization of geometrically nonlinear structures could be of significant benefit because of its high computational efficiency and lack of intermediate-density elements in the solutions, while it still benefits from high-resolution boundary representation. In the next sections of this article, after presenting an overview of the Iso-XFEM method, a nonlinear modelling strategy for geometrically nonlinear structures based on an incremental–iterative Newton–Raphson approach is presented. An appropriate structural performance criterion for stiffness design is derived and the Iso-XFEM method is demonstrated for several large-deformation problems.

2. Overview of the Iso-XFEM method

The main three elements of the Iso-XFEM method are an isoline/isosurface approach to represent the design boundary, XFEM to calculate the elemental sensitivities (a structural performance criterion) near the boundary, and an evolutionary-based optimization algorithm. These three elements are explained in this section.

2.1. Isoline/isosurface approach

Isolines/isosurfaces are the lines/surfaces that represent the points at which a function has a constant value, named the isovalue, in a 2D/3D space. In structural optimization applications (Abdi, Wildman, and Ashcroft 2014; Abdi, Ashcroft, and Wildman 2014; Victoria, Martí, and Querin 2009; Victoria, Querin, and Martí 2010), the boundaries are defined by the intersection of the structural performance (SP) distribution with a minimum level of performance (MLP), which typically increases during the optimization process. Figure 1(a) shows a 2D fixed grid design domain discretized with a 30×30 mesh, where the intersection of SED distribution as a structural performance criterion with a minimum level of SED gives the design boundary. The relative performance, α, is defined as

$$\alpha = SP - MLP \tag{1}$$

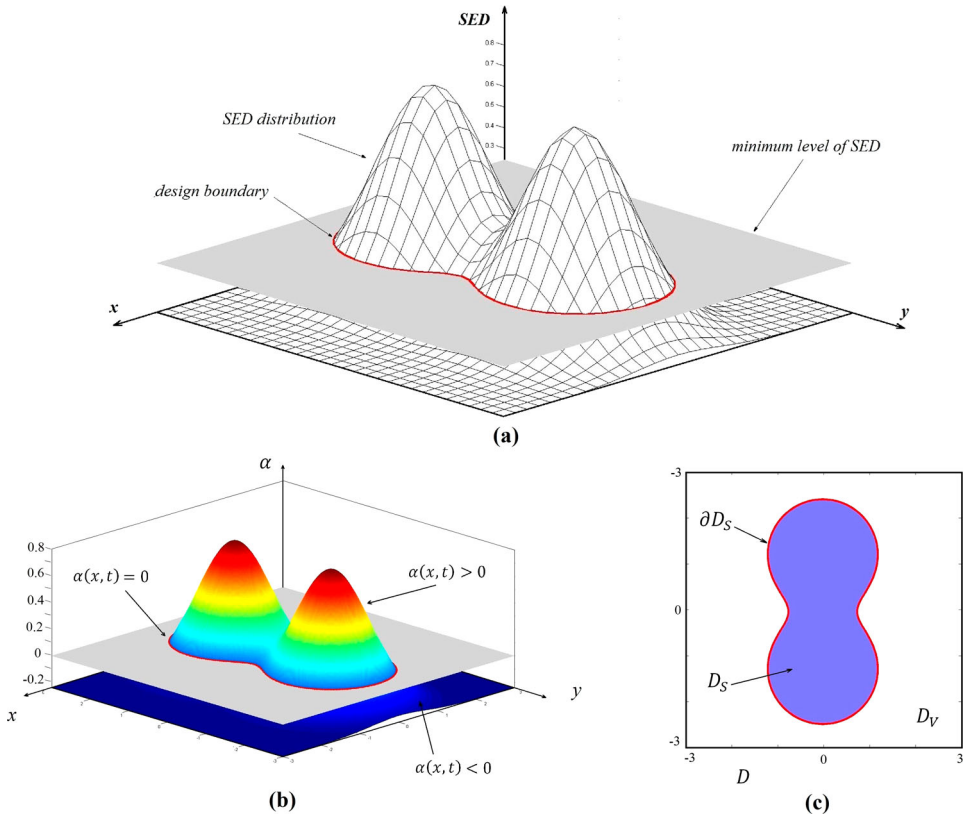

Figure 1. (a) Boundary representation using isolines of a structural performance (SP) function [strain energy density (SED)]. The intersection of SP distribution with the minimum level of performance (MLP) defines the current state of the boundary. (b) Implicit representation of a two-dimensional design space and the structure's geometry using relative structural performance (α). (c) Design space decomposed into the solid region ($\alpha(x) > 0$), void region ($\alpha(x) < 0$) and boundary ($\alpha(x) = 0$).

The design domain can be partitioned into the void phase, boundary and solid phase, with respect to the values of relative performance:

$$\alpha(x) : \begin{cases} > 0 & \text{solid phase} \quad (D_S) \\ = 0 & \text{boundary} \quad (\partial D_S) \\ < 0 & \text{void phase} \quad (D_V) \end{cases} \tag{2}$$

Figure 1(b) and (c) shows how the design space, D, from Figure 1(a) is partitioned into D_S, ∂D_S and D_V using the relative performance function $\alpha(x)$, distributed over the design space.

2.2. XFEM

By implementing the above isoline/isosurface approach, the design boundary is superimposed on the fixed grid FEs, making three groups of elements in the FE design space: solid elements, void elements and boundary elements (the elements that lie on the boundary). The contribution of solid and void elements to the FE framework can simply be considered by assigning solid and void (very weak) material properties to those elements, respectively. In the case of boundary elements, to accurately represent the design boundary while avoiding expensive remeshing operations, an XFEM approach can be employed. An XFEM displacement function for modelling holes and inclusions is given by

(Sukumar *et al.* 2001)

$$u(x) = \sum_i N_i(x)H(x)u_i \tag{3}$$

where $N_i(x)$ are the classical shape functions associated with the nodal degrees of freedom, u_i. The value of the Heaviside function $H(x)$ is equal to 1 for the nodes and regions in the solid part of the design and switches to 0 for nodes and regions in the void part of the design domain. Based on the above displacement function, the stiffness matrix of an element with material–void discontinuity is given by (Sukumar *et al.* 2001)

$$k_e = \int_\Omega B^T \mathrm{CH}(x) B \mathrm{d}\Omega \tag{4}$$

where Ω is the element domain, B is the displacement differentiation matrix, and C is the elasticity matrix for the solid material. This XFEM scheme was realized by dividing the solid domain of the boundary elements into sub-triangles (in 2D problems as shown in Figure 2(a)) or sub-tetrahedra (in 3D problems as shown in Figure 2(b)), and then performing numerical integration over solid triangles/tetrahedra using the Gauss quadrature method (Abdi, Ashcroft, and Wildman 2014).

The XFEM decomposition scheme shown in Figure 2 requires finding the solid domain of boundary elements before decomposing it into triangles/tetrahedra. The solid domain of a boundary element can be defined using solid nodes of the element (nodes with positive values of relative performance) and the intersection points of the element edges and the boundary, *i.e.* points with zero value of relative performance which can be found through bilinear (in 2D) or trilinear (in 3D) interpolation of relative performance (α) between the nodes. Various decomposition schemes can then be employed to define sub-triangles/sub-tetrahedra for numerical integration, resulting in a similar numerical accuracy (Li, Wang, and Wei 2012). For instance, the solid region of quadrilateral elements in Figure 2(a) was decomposed into sub-triangles by connecting a central point of the solid region to the surrounding solid nodes and intersection points. Similarly, a hexahedral element can be initially decomposed to a number of tetrahedra. For those tetrahedra that lie on the boundary, the solid region of the tetrahedra can be further decomposed into sub-tetrahedra (Figure 2(b)), with the numerical integration being performed over all solid tetrahedra.

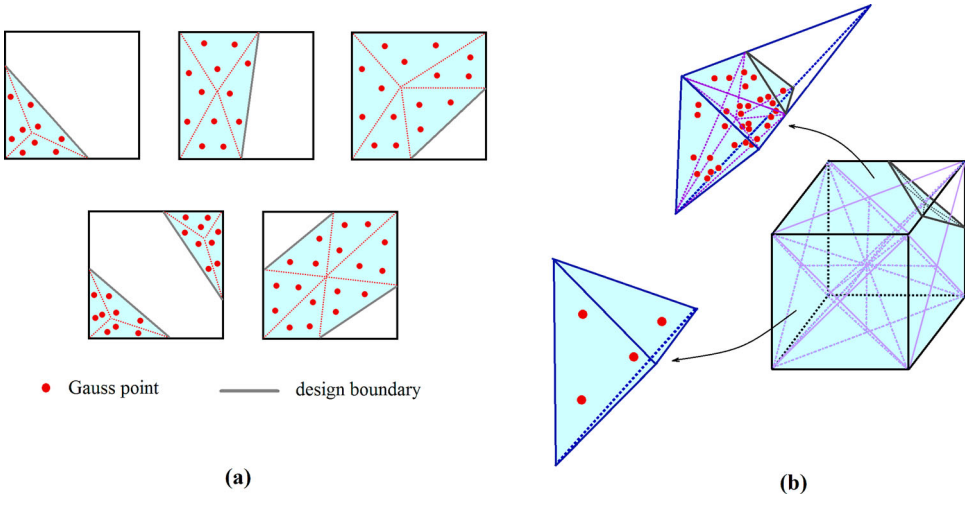

Figure 2. Extended finite element method (XFEM) integration scheme: (a) solid domain of two-dimensional boundary elements, divided into sub-triangles; (b) solid domain of 3D boundary elements, divided into sub-tetrahedra.

2.3. Evolutionary-based optimization method

The optimization algorithm used in the Iso-XFEM method is evolutionary based, *i.e.* based on the simple assumption that the optimized solution can be achieved by gradually removing the inefficient material from the design domain. However, unlike ESO, in which the material removal is carried out at an elemental level, in this approach the optimization operates at a global level of structural performance by the use of an isoline/isosurface design approach. An appropriate performance criterion is used to characterize the efficiency of material usage in the design domain. Material is then removed from low relative performance regions ($x; \alpha(x) < 0$) and redistributed to the high relative performance regions ($x; \alpha(x) > 0$). The target volume of the design for the current iteration needs to be calculated before any region is added to or removed from the structure. The target volume of the design for the current iteration is given by

$$V_{it} = \max(V_{it-1}(1 - ER), V^c) \tag{5}$$

where ER is the volume evolution rate and V^c is the specified volume constraint. Once the target volume of the current iteration is found, the minimum level of performance that gives this volume needs to be identified. This could be achieved through an iterative process, for instance by defining upper and lower bands for MLP (which are equal to the maximum and minimum structural performance in the first iteration, respectively), finding the volumes corresponding to the upper and lower bands, averaging and updating the upper and lower bands until the difference between the volumes corresponding to the upper and lower bands is smaller than a minimum value. The evolutionary process continues until the volume fraction condition is satisfied. From this time forwards, the optimization process runs with a constant volume fraction (as given by Equation 5) until the changes in the objective function in the last five iterations are within a specified tolerance.

Figure 3 compares solutions achieved using SIMP, BESO and Iso-XFEM for the cantilever problem of Figure 3(a) assuming linear deformations. It can be seen that the Iso-XFEM solution (Figure 3(d)) is represented with clearly defined boundaries, unlike the SIMP (Figure 3(b)) and BESO (Figure 3(c)) solutions, in which the solutions are represented with variable element densities and/or background mesh-defined boundaries. A more in-depth comparison of the methods in terms of solution

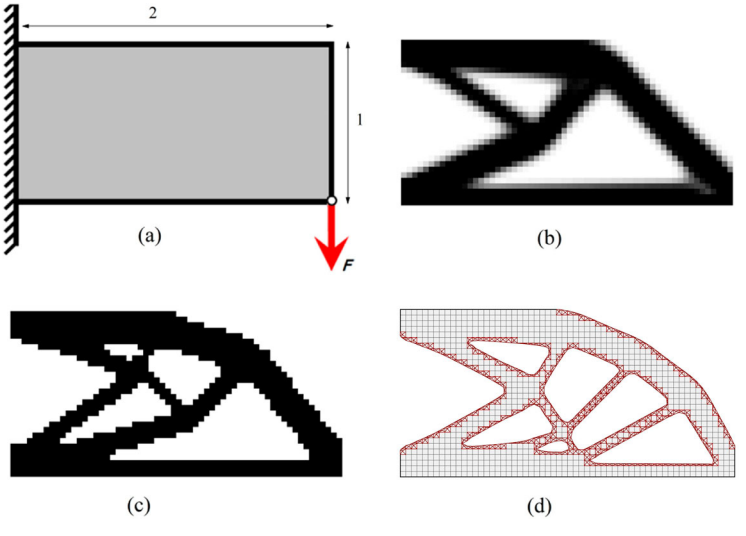

Figure 3. Comparison of topology optimization solutions achieved using different methods assuming linear deformation: (a) design domain; (b) solid isotropic material with penalization (SIMP) solution; (c) bidirectional evolutionary structural optimization (BESO) solution; (d) topology optimization using isolines/isosurfaces and extended finite element method (Iso-XFEM) solution.

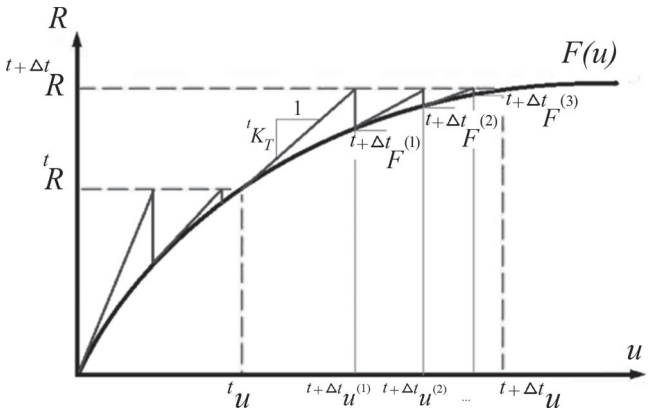

Figure 4. Illustration of the incremental Newton–Raphson approach.

performance can be found in Abdi, Wildman, and Ashcroft (2014) and Abdi, Ashcroft, and Wildman (2014).

3. Modelling geometric nonlinearity

3.1. Incremental–iterative approach

In this study, the incremental Newton–Raphson approach is utilized to find the equilibrium solution at every evolutionary iteration. In this approach, the applied load (R) is first divided into a set of smaller load increments. Then, starting from the first load increment, using the tangent stiffness matrix (K_T), the displacement caused by that force increment is computed. Using the accumulated displacement, the resistant force (F) is obtained and the unbalanced force (${}^{t}R - {}^{t}F$), which is the difference between the applied and the resistant forces, is determined. The iterative process at this load increment continues by calculating a new tangent stiffness matrix, finding the displacement and the unbalanced force (Figure 4). The equations used in the Newton–Raphson method can be stated as (Bathe 2006)

$$\begin{aligned} {}^{t+\Delta t}K_T^{(it-1)}\,\Delta u^{(it)} &= {}^{t+\Delta t}R - {}^{t+\Delta t}F^{(it-1)} \\ {}^{t+\Delta t}u^{(it)} &= {}^{t+\Delta t}u^{(it-1)} + \Delta u^{(it)} \end{aligned} \tag{6}$$

where Δt is a suitably chosen time increment and it denotes the iteration number of the Newton–Raphson procedure in each time increment. The initial conditions at the start of each time increment are:

$${}^{t+\Delta t}u^{(0)} = {}^{t}u; \quad {}^{t+\Delta t}K_T^{(0)} = {}^{t}K_T; \quad {}^{t+\Delta t}F^{(0)} = {}^{t}F \tag{7}$$

Convergence is achieved when both the errors, measured as the Euclidean norms of the unbalanced forces and of the residual displacements, are less than a minimum value. The complete equilibrium path can be traced by finding the subsequent solution points at higher load levels using the same approach.

3.2. Geometrically nonlinear behaviour of a continuum body

In this study, the assumption is that the structures undergo large deformation with small strain. To model this nonlinear behaviour, the total Lagrangian (TL) formulation is utilized, in which all static and kinematic variables are referred to the initial undeformed configuration of the structure and the integrals are calculated with respect to that configuration. Because of the transformations,

a new measure for stress, the second Piola–Kirchhoff stress tensor, has to be introduced with the Green–Lagrange strain tensor. Considering TL formulation for a general body subjected to applied body forces f^B and surface tractions f^S on the surface S and displacement field δu_i, the equation of motion is given by (Gea and Luo 2001)

$$\int_{{}^0V} S_{ij}\delta\epsilon_{ij}d^0V = \int_{{}^0V} f_i^B\delta u_i d^0V + \int_{{}^0S_f} f_i^S\delta u_i{}^S d^0S \tag{8}$$

where S_{ij} denote the Cartesian components of the second Piola–Kirchhoff stress tensor, $\delta\epsilon_{ij}$ are the components of the Green–Lagrange strain tensor corresponding to the virtual displacement field δu_i, and ${}^0V$ denotes the body volume at initial configuration. The Green–Lagrange strain tensor, which is defined with respect to the initial configuration of the body, is given by (Gea and Luo 2001)

$$\epsilon_{ij} = \frac{1}{2}\left(\frac{\partial u_i}{\partial {}^0x_j} + \frac{\partial u_j}{\partial {}^0x_i} + \frac{\partial u_k}{\partial {}^0x_i}\frac{\partial u_k}{\partial {}^0x_j}\right) \tag{9}$$

Considering reasonably small strains, the general elastic constitutive equation can still be used:

$$S_{ij} = C_{ijkl}\epsilon_{ij} \tag{10}$$

where C is the elasticity tensor. Equations (8)–(10) are the basic equations for calculating the response of a continuum body using the TL formulation. However, to solve these equations for strongly nonlinear problems, one may need to use an incremental–iterative approach, such as Newton–Raphson, as discussed in Section 3.1.

3.3. Continuous form of the equilibrium equation

Introducing the incremental approach to find the structural responses in nonlinear structures, one can decompose the displacements, strains and stresses at time $t + \Delta t$ as

$${}^{t+\Delta t}u_i = {}^t u_i + \Delta u_i; \quad {}^{t+\Delta t}\epsilon_{ij} = {}^t\epsilon_{ij} + \Delta\epsilon_{ij}; \quad {}^{t+\Delta t}S_{ij} = {}^tS_{ij} + \Delta S_{ij} \tag{11}$$

where Δu_i, $\Delta\epsilon_{ij}$ and ΔS_{ij} denote the displacements, strains and stresses increments, respectively, to be determined. The strain increments can be defined as the sum of linear and nonlinear terms as

$$\Delta\epsilon_{ij} = e_{ij} + \eta_{ij} \tag{12}$$

where the linear incremental strain, e_{ij} is given by

$$e_{ij} = \frac{1}{2}\left(\frac{\partial\Delta u_i}{\partial {}^0x_j} + \frac{\partial\Delta u_j}{\partial {}^0x_i} + \frac{\partial\Delta u_k}{\partial {}^0x_j}\frac{\partial {}^t u_k}{\partial {}^0x_i} + \frac{\partial\Delta u_k}{\partial {}^0x_i}\frac{\partial {}^t u_k}{\partial {}^0x_j}\right) \tag{13}$$

and the nonlinear incremental strain, η_{ij} is defined by

$$\eta_{ij} = \frac{1}{2}\frac{\partial\Delta u_k}{\partial {}^0x_i}\frac{\partial\Delta u_k}{\partial {}^0x_j} \tag{14}$$

Implementing Equation (11) into the equilibrium equation (Equation 8) and assuming $\Delta S_{ij} = C_{ijkl}e_{ij}$ and $\delta\Delta\epsilon_{ij} = \delta e_{ij}$, the linearized incremental equation of motion is obtained as

$$\int_{{}^0V} c_{ijkl}e_{ij}\delta e_{kl}d^0V + \int_{{}^0V} {}^tS_{ij}\delta\eta_{ij}d^0V = \int_{{}^0V} {}^{t+\Delta t}f_i^B\delta\Delta u_i d^0V + \int_{{}^0S_f} {}^{t+\Delta t}f_i^S\delta\Delta u_i^S d^0S - \int_{{}^0V} {}^tS_{ij}\delta e_{ij}d^0V \tag{15}$$

The left-hand side of Equation (15), which is dependent on the displacements and stress field, defines the so-called tangent structure. The right-hand side of this equation represents the out-of-balance virtual work of the body. One may need to use iterative methods for solving this equation until the out-of-balance force vanishes.

3.4. Finite element formulation

Transforming the continuous form of the equation of motion represented by Equation (15) to an FE formulation, the equilibrium equation is obtained as (Gea and Luo 2001; Bathe 2006)

$$ {}^{t}K_T \Delta U = (K_0 + K_d + K_\sigma)\Delta U = \Delta F \tag{16} $$

where ${}^{t}K_T$ is the tangent stiffness matrix and ΔF is the load imbalance between the external forces ${}^{t+\Delta t}R$ and the internal forces ${}^{t}F$. K_0 is the usual small displacement stiffness matrix represented by

$$ K_0 = \int_{V_0} B_{L0}^T C B_{L0} d^0 V \tag{17} $$

where B_{L0} is a linear strain–displacement transformation matrix used in linear infinitesimal strain analysis. The stiffness matrix K_d in Equation (16) represents the large displacement stiffness matrix and is defined by

$$ K_d = \int_{V_0} (B_{L0}^T C B_{L1} + B_{L1}^T C B_{L0} + B_{L1}^T C B_{L1}) d^0 V \tag{18} $$

where B_{L1} is a linear strain–displacement transformation matrix which depends on the displacement. K_σ in Equation (16) is the initial stress matrix dependent on the stress level, and is given by

$$ K_\sigma = \int_{V_0} B_{NL}^T {}^{t}S B_{NL} d^0 V \tag{19} $$

where B_{NL}^T denotes the nonlinear strain–displacement transformation matrix and ${}^{t}S$ denotes the second Piola–Kirchhoff stress matrix, which in a 2D formulation is defined by

$$ {}^{t}S = \begin{bmatrix} {}^{t}S_{11} & {}^{t}S_{12} & 0 & 0 \\ {}^{t}S_{21} & {}^{t}S_{22} & 0 & 0 \\ 0 & 0 & {}^{t}S_{11} & {}^{t}S_{12} \\ 0 & 0 & {}^{t}S_{21} & {}^{t}S_{22} \end{bmatrix} \tag{20} $$

The correct calculation of the internal forces, ${}^{t}F$ in Equation (16), is crucial as any error in this calculation will result in an inaccurate response prediction. The internal forces can be found from

$$ {}^{t}F = \int_{V_0} (B_{L0} + B_{L1})^T {}^{t}\bar{S} d^0 V \tag{21} $$

where ${}^{t}\bar{S}$ is the second Piola–Kirchhoff stress vector. Equation (16) is used to find the displacement increment corresponding to the state $t + \Delta t$, which is then added to the displacement at state t to obtain displacement at state $t + \Delta t$. The strain–displacement relation in Equation (9) allows the strain to be determined from the displacements and, using the constitutive relation in Equation (10), one can then calculate the corresponding stresses.

3.5. XFEM for geometrically nonlinear behaviour

To find the properties of the elements on the evolving boundary during the optimization process, a similar XFEM scheme as in the linear case (Section 2.2) can be used. In the case of geometrically nonlinear problems, the contributions of the solid parts of the boundary elements into the elements' tangent stiffness matrix as well as the elements' internal forces need to be identified. Therefore, the integrations associated with tangent stiffness matrix (Equations 17–19) and internal forces (Equation

21) should be merely performed on the solid region of a boundary element. If four-node quadrilateral elements are used in the FE model of the structure, this can be done by dividing the solid part of the boundary elements into sub-triangles and performing Gauss quadrature (Abdi, Ashcroft, and Wildman 2014). Following that, the element's tangent stiffness matrix ${}^{t}k_T$ can be obtained from

$$ {}^{t}k_T = \sum_{i=1}^{n}\sum_{j=1}^{m} A_i t w_j f_1(\xi_1^j, \xi_2^j, \xi_3^j) \tag{22} $$

where i and j are the indices regarding the partitions and Gauss points, respectively; n is the number of solid partitions (sub-triangles) inside the element and m is the number of Gauss points in each partition. $\xi_{1:3}$ are the natural coordinates of the Gauss points, A_i is the area of the triangle i, t is the thickness of the 2D element, w is a weighting factor and

$$ f_1 = B^T C B + B_{L0}^T C B_{L1} + B_{L1}^T C B_{L0} + B_{L1}^T C B_{L1} + B_{NL}^T {}^{t}S B_{NL}. \tag{23} $$

Internal force vector ${}^{t}F_e$ can be obtained from

$$ {}^{t}F_e = \sum_{i=1}^{n}\sum_{j=1}^{m} A_i t w_j f_2(\xi_1^j, \xi_2^j, \xi_3^j) \tag{24} $$

where

$$ f_2 = (B_{L0} + B_{L1})^T {}^{t}\bar{S} \tag{25} $$

The elements' tangent stiffness matrices and internal force vectors can then be assembled to obtain the global tangent stiffness matrix ${}^{t}K_T$ and global internal force vector ${}^{t}F$ of the structure.

4. Stiffness design

4.1. Objective function and structural performance criteria

To find the stiffest design, the natural choice is to minimize the deflection or compliance. However, the drawback of this objective function is that it may result in structures that can only support the maximum load for which they are designed and may break down for lower loads (Buhl, Pedersen, and Sigmund 2000). To avoid this, when the nonlinear structure is loaded under force control, the complementary work W^C can be chosen as the objective function (Figure 5). In this case, the optimization problem can be defined as:

$$ \begin{aligned} &\text{Minimize}: f(x) = W^C = \lim_{n\to\infty} \tfrac{1}{2} \sum_{i=1}^{n} \Delta R^T (U_i - U_{i-1}) \\ &\text{subject to}: \sum_{e=1}^{n} v_e^s = V^c \end{aligned} \tag{26} $$

where ΔR is the load increment, i denotes the increment number, and n is the total number of load increments.

The sensitivity of the objective functions with respect to design variable x_e is:

$$ S_e = \frac{\partial f(x)}{\partial x_e} = \lim_{n\to\infty} \frac{1}{2} \sum_{i=1}^{n} (R_i^T - R_{i-1}^T) \left(\frac{\partial U_i}{\partial x_e} - \frac{\partial U_{i-1}}{\partial x_e} \right) \tag{27} $$

To find the elemental sensitivities, an adjoint equation was introduced to the above equation by adding a series of Lagrangian multipliers to the objective function (Buhl, Pedersen, and Sigmund 2000).

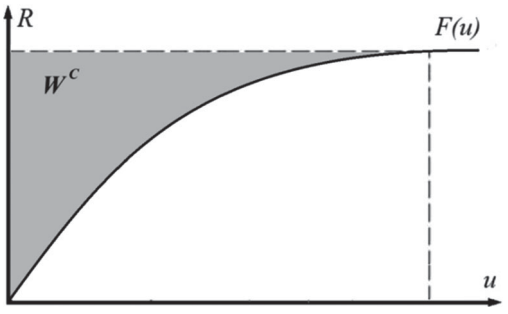

Figure 5. Objective function W^C for stiffness optimization of nonlinear structures under force control.

Solving the above equation, the elemental sensitivity numbers for nonlinear structures under force control are obtained as the total elemental elastic and plastic strain energy, E_e^n (Huang and Xie 2010). This can be used in BESO as the criterion for element removal and addition to find the solution for stiffness optimization of nonlinear structures. Similarly, in the Iso-XFEM optimization method, the elemental sensitivity numbers can be used to find the structural performance:

$$SP_e = \frac{E_e^n}{V_e} \tag{28}$$

4.2. Filter scheme for Iso-XFEM

To increase the stability of the Iso-XFEM method applied to geometrically nonlinear problems, a similar filter scheme to the one used for BESO (Huang and Xie 2010) and SIMP (Sigmund 2001) can be employed. Here, the purpose of the filter is to smooth the structural performance distribution over the design domain by averaging the nodal values of structural performance with those of neighbouring nodes. The modified values of structural performance can then be defined by

$$SP_i = \frac{\sum_{j=1}^{k} w_{ij} SP_j}{\sum_{j=1}^{k} w_{ij}} \tag{29}$$

where k is the number of nodes inside a domain centred at node i having a filter radius of $r_{\min}$, and w_{ij} are the weighting factors defined by

$$w_{ij} = r_{\min} - r_{ij} \tag{30}$$

where r_{ij} is the distance between node i and the neighbouring node j.

4.3. Iso-XFEM procedure for geometrically nonlinear structures

The Iso-XFEM procedure for stiffness design of geometrically nonlinear structures can be summarized as the following steps, as also illustrated in Figure 6.

- Initialize: define the design space, non-design domain, material properties, a fixed grid FE mesh, loads and boundary conditions, and the optimization parameters.
- Perform nonlinear finite element analysis (FEA): divide the applied load into a suitable number of load increments and find the equilibrium path using the Newton–Raphson approach. Find the properties of the boundary elements using the XFEM scheme.
- Calculate the elemental values of total strain energy and find the structural performance distribution over the design domain.

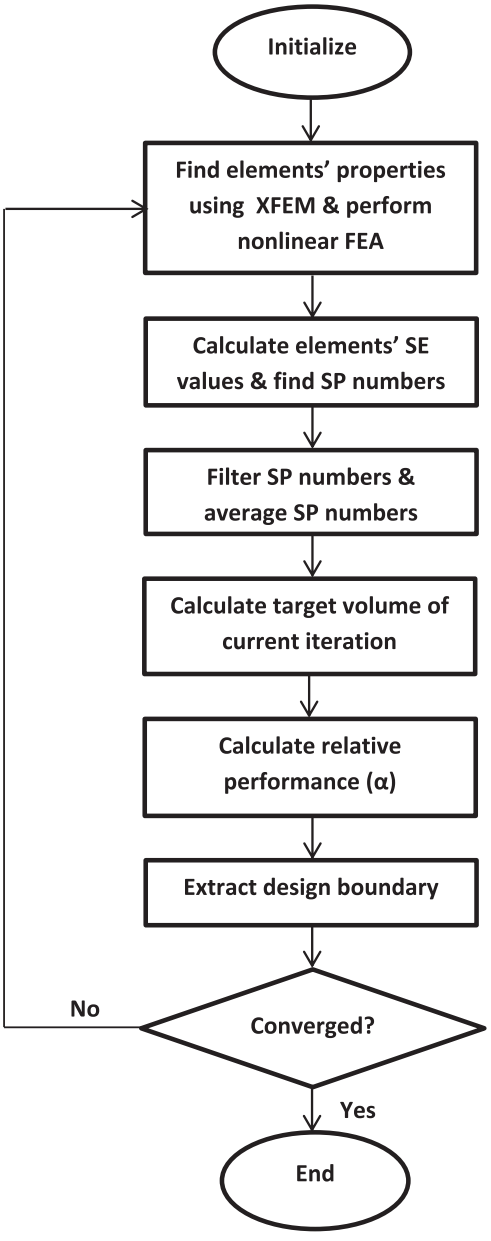

Figure 6. Flowchart of the extended finite element method using isolines/isosurfaces (Iso-XFEM) for geometrically nonlinear structures. XFEM = extended finite element method; FEA = finite element analysis; SE = strain energy; SP = structural performance.

- Filter structural performance numbers.
- Average the structural performance numbers with those of the previous iteration.
- Calculate the target volume of the current iteration and find a minimum level of performance to meet the target volume.
- Find the relative performance, α, over the design domain and extract the design boundary. Assign solid material properties to regions having $\alpha > 0$ and void material properties to the regions having $\alpha < 0$.
- If the convergence condition is reached, stop the design process; else, go to Step 2.

5. Examples

5.1. Test case 1: nonlinear cantilever plate

The cantilever plate shown in Figure 7 was considered as the first test case of this study. This beam has been used as a test case in previous studies, implementing SIMP (Buhl, Pedersen, and Sigmund 2000) and BESO (Huang and Xie 2010), allowing comparison of the Iso-XFEM solutions with the other two methods. The cantilever plate was 1 m in length, 0.25 m in width and 0.1 m in thickness, and was subjected to a concentrated load at the middle of the free end. The material used was nylon, which has a Young's modulus of $E = 3$ GPa and Poisson's ratio of $\nu = 0.4$. Nonlinear, stiffness-optimized designs of the plate with a volume constraint of 50% of the design domain under two point loads 60 kN and 144 kN were investigated and compared. A mesh of 200×50 quadrilateral elements was used for the FE model of the structure. A relatively low evolution rate of $ER = 0.005$ was used to increase the stability of the nonlinear Iso-XFEM method by performing the material removal within a higher number of evolutionary iterations, *i.e.* applying less change to the topology at each iteration. A filter radius of $r_{\min} = 1.2$ times the element size was used. The reason for using a small filter radius was to stabilize the evolutionary process without significantly changing the complexity of the solutions.

Figure 8 shows the evolution histories of the objective function (W^C) and volume fraction for both load cases, 60 kN and 144 kN. It can be seen that the evolutionary optimization process of the nonlinear structure subjected to the point load of 60 kN (Figure 8(a)) has good stability. However, by increasing the load to 144 kN (Figure 8(b)), *i.e.* increasing the degree of nonlinearity, some instability was observed in the plot of complementary work (iteration 70 afterwards). Figure 9 shows the solutions obtained from the linear and nonlinear optimization for the two different load values. Note that linear Iso-XFEM solutions for both load cases are the same when the same target volume fraction is used. It can be seen that the linear Iso-XFEM has converged to a symmetrical solution. This is expected as the design is optimized with respect to the equilibrium geometry of the undeformed beam. However, different designs are obtained by implementing the nonlinear topology design, showing that the optimal topologies depend on the magnitude of the applied load. These are now non-symmetrical as the design is optimized for the deformed beam under load, which is not symmetrical. The large deformation of the Iso-XFEM solutions is illustrated in Figure 10. Table 1 compares the objective values (complementary works) of the linear and nonlinear Iso-XFEM solutions with those previously investigated using SIMP (Buhl, Pedersen, and Sigmund 2000) and BESO (Huang and Xie 2010), implementing the same objective function. It can be seen that the nonlinear designs obtained from both Iso-XFEM designs have lower magnitudes of complementary work than their linear designs, indicating a better performance for the load for which they are designed. Also comparing the Iso-XFEM with BESO and SIMP solutions in terms of their complementary work, it can be seen that the Iso-XFEM solutions have lower magnitudes of complementary work than the BESO and SIMP solutions, showing better performance of the Iso-XFEM solutions owing to their smooth boundary representation. The slightly higher complementary work of the SIMP solutions compared to the BESO solutions was attributed to the effect of intermediate-density elements in SIMP

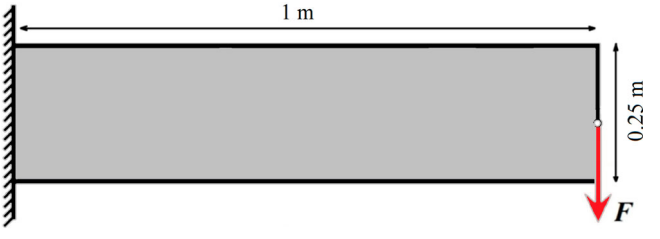

Figure 7. Design domain and boundary conditions of the geometrically nonlinear cantilever plate.

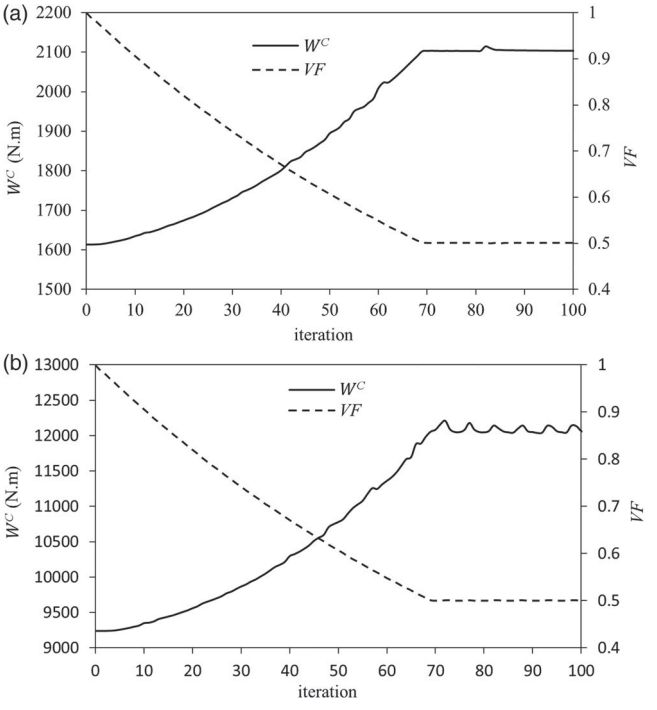

Figure 8. Evolution histories of the objective function and volume fraction of the nonlinear cantilever subjected to a point load of (a) 60 kN, and (b) 144 kN.

Table 1. Comparison of the complementary works of linear and nonlinear designs for test case 1.

Complementary work	Design for $F = 60$ kN	Design for $F = 140$ kN
Linear design from Iso-XFEM	2.107 kJ	12.072 kJ
Nonlinear design from Iso-XFEM	2.101 kJ	12.063 kJ
Nonlinear design from BESO (Huang and Xie 2010)	2.171 kJ	12.38 kJ
Nonlinear design from SIMP (Buhl, Pedersen, and Sigmund 2000)	2.331 kJ	13.29 kJ

Note: Iso-XFEM = topology optimization using isolines/isosurfaces and extended finite element method; BESO = bidirectional evolutionary structural optimization; SIMP = solid isotropic material with penalization.

solutions, where their strain energy may have been overestimated (Huang and Xie 2010). This cantilever problem has also been studied for compliance minimization (Buhl, Pedersen, and Sigmund 2000; He, Kang, and Wang 2014). In this case, a different solution with a tail member was reported. However, as pointed out by Buhl, Pedersen, and Sigmund (2000) and Huang and Xie (2010), the solutions achieved from minimizing compliance may not support a load lower than the maximum load for which they are designed.

The test case presented in this section shows that by using nonlinear FE modelling in the Iso-XFEM method, a different solution with a higher performance than the linear design can be achieved. However, it could be argued that the difference in the overall topology of the linear and nonlinear solutions of this test case was insufficient to justify the extra effort of the nonlinear analysis. As will be shown in the next example, in some cases the difference can be extremely large and can make the use of nonlinear modelling essential.

5.2. Test case 2: slender beam

The purpose of this experiment was to apply the Iso-XFEM method to the topology optimization of a structure having snap-through buckling effects, *i.e.* a transition between two stable states in a

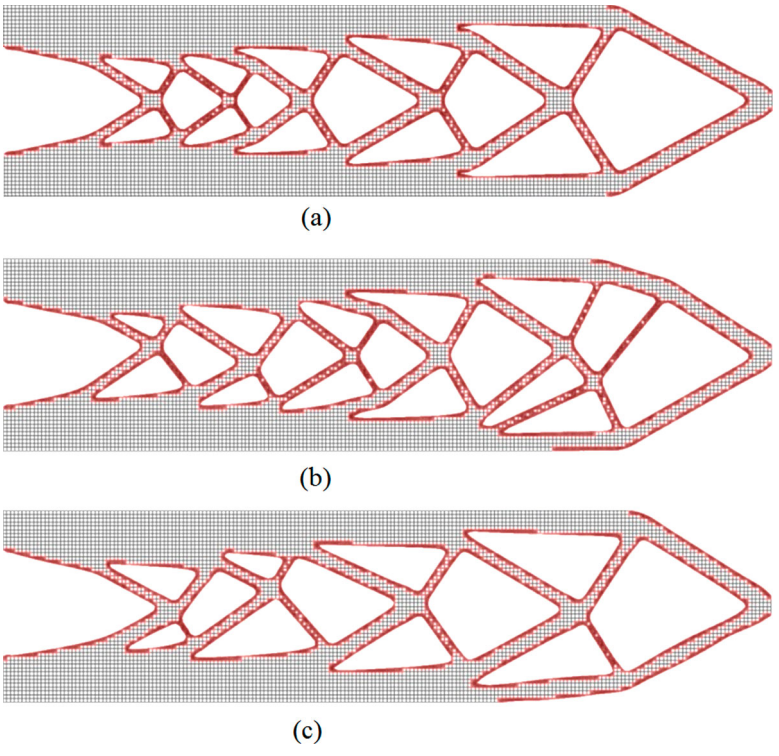

Figure 9. Extended finite element method using isolines/isosurfaces (Iso-XFEM) solutions of the large-displacement cantilever problem: (a) linear design (for both load cases of 60 kN and 144 kN); (b) nonlinear design for a point load of 60 kN; (c) nonlinear design for a point load of 144 kN.

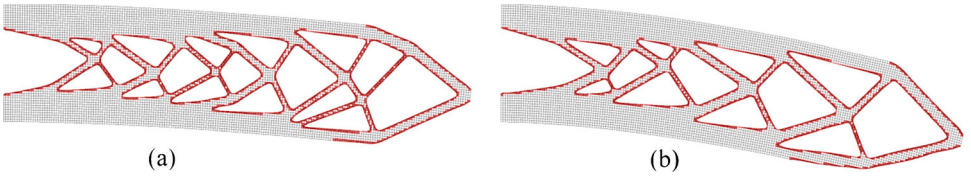

Figure 10. Illustration of the large deformation of the cantilever plate: (a) cantilever subjected to a point load of 60 kN; (b) cantilever subjected to a point load of 144 kN. The deformations are to scale.

structure. In this type of problem, radically different topologies can be obtained using linear and nonlinear modelling in the structural optimization problem. As an example of a structure involving snap-through effects, the topology optimization of a slender beam with the design domain and boundary conditions shown in Figure 11 was considered. The beam was 8 m long, 1 m deep and 100 cm thick. A load of 400 kN was applied to the centre of the top edge The material properties of the beam were a Young's modulus of $E = 3$ GPa and Poisson's ratio of $\nu = 0.4$. Nonlinear and linear stiffness-optimized designs of the beam for a volume constraint of 20% of the design domain for downward and upward loads were investigated. A mesh of 320×40 quadrilateral elements was used for the FE model of the structure in all the experiments, and a volume evolution rate of $ER = 0.01$ and a filter radius of $r_{\min} = 1.2$ times the element size were used as optimization parameters.

Figure 12 compares the nonlinear Iso-XFEM solutions of the beam subjected to downward (Figure 12(a)) and upward (Figure 12(b)) loads with the linear Iso-XFEM solution (Figure 12(c)). With the linear modelling, the same solution is obtained for the structure subjected to either an

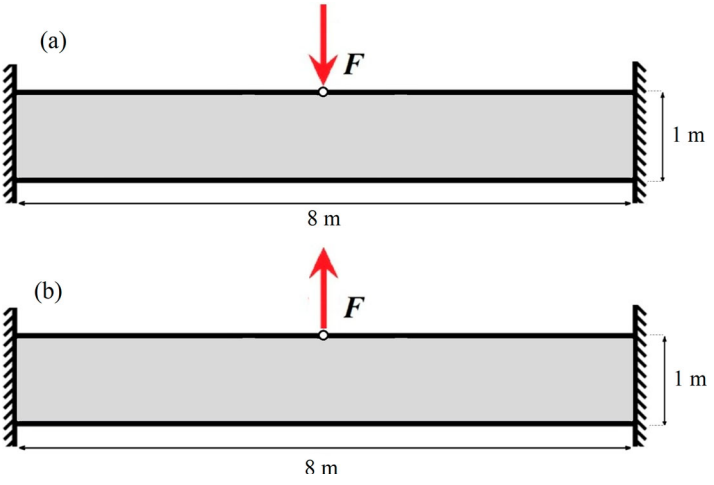

Figure 11. Design domain and boundary conditions of the geometrically nonlinear slender beam of test case 2: (a) beam subjected to downward load; (b) beam subjected to upward load.

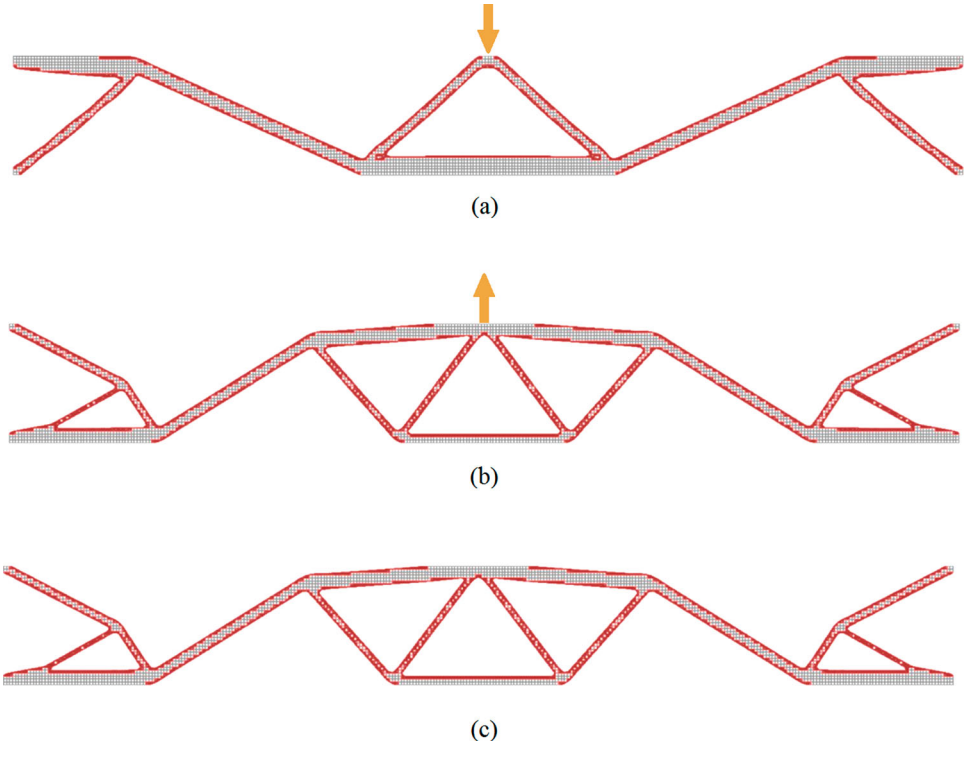

Figure 12. (a) Nonlinear design of the beam subjected to a downward load; (b) nonlinear design of the beam subjected to an upward load; (c) linear design of the beam (for both downward load and upward load cases).

upward or a downward load, *i.e.* the magnitude of the load does not change the solution in a linear topology optimization implementation. However, it can be seen that, using the nonlinear topology design approach, very different solutions are obtained for upward and downward loads. It can also be seen in Figure 12 that the solution for the upward load case is very similar to the linear solution. This can be explained by looking at the deformations of the various designs under load.

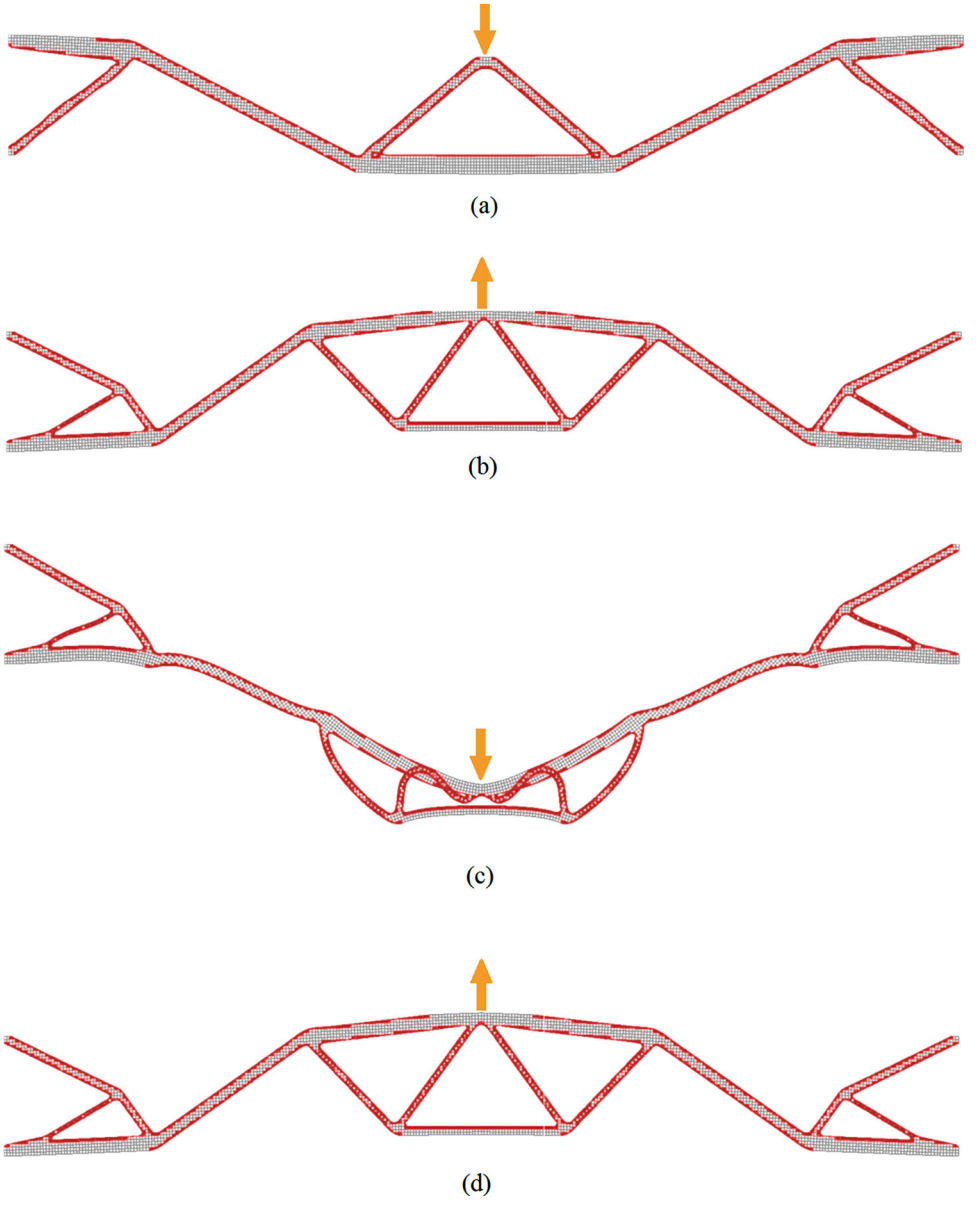

Figure 13. (a) Displacement of solution shown in Figure 12(a); (b) displacement of solution shown in Figure 12(b); (c) displacement of solution shown in Figure 12(c) subjected to downward load; (d) displacement of solution shown in Figure 12(c) subjected to upward load. The deformations are to scale.

Figure 13 shows the deflection of the nonlinear and linear topology optimization solutions of the beam, subjected to both upward and downward loads. The deflection of both nonlinear and linear solutions was determined using geometrically nonlinear FEA for this comparison. It can be seen that the solution of the nonlinear design subjected to the downward load remains stable after applying the specified load for which it is designed (Figure 13(a)). However, the linear design has become distorted under the prescribed downward load (Figure 13(c)), which can be attributed to the buckling effects (Buhl, Pedersen, and Sigmund 2000). This is because the linear solution of Figure 12(c) has two thin members in the middle which are put under compression with the downward load. Although this

Table 2. Comparison of the complementary works of nonlinear and linear designs for test case 2.

Complementary work	Design for downward load	Design for upward load
Nonlinear design from Iso-XFEM	38.700 kJ	36.492 kJ
Linear design from Iso-XFEM	55.548 kJ	36.494 kJ

Note: Iso-XFEM = topology optimization using isolines/isosurfaces and extended finite element method.

is not an issue when linear modelling is used, with nonlinear modelling the thin compressed beams buckle and the whole structure experiences snap-through, as seen in Figure 13(c). The snap-through effect was not an issue for the upward loading as the thin struts were not put under compression, hence the similarity of the linear and nonlinear designs for upward loading (Figure 13(b) and (d)). Table 2 compares the complementary works of the solutions subjected to downward and upward loads. As anticipated, the difference between the complementary works of nonlinear and linear solutions for the upward load case is not significant. However, in the case of the downward load case, the complementary work of the linear design involving buckling and snap-through effects is much higher than for the nonlinear one, showing the importance of implementing a nonlinear topology optimization approach for large-displacement problems such as those involving snap-through effects.

5.3. Further remarks on the efficiency of the proposed method

The test cases studied in this article showed how the Iso-XFEM method can benefit from nonlinear modelling, especially when the method is applied to problems with a high degree of geometric nonlinearity. However, it should be noted that the computational cost of optimization significantly increases when nonlinear modelling is used. For example, in test case 1, the time cost of the optimization with linear modelling was 3020 s for 100 iterations. Using the same desktop computer for the analysis, the corresponding time cost for optimization of the cantilever under 140 kN load with nonlinear modelling was 15,895 s for 100 iterations. The increased computational cost of nonlinear modelling can become problematic when applying the method to 3D problems with a high number of FEs. However, compared to conventional element-based methods of topology optimization, an advantage of the Iso-XFEM method is that it requires fewer elements to return a high-resolution solution, thus saving on the computational cost of the optimization (Abdi, Wildman, and Ashcroft 2014; Abdi, Ashcroft, and Wildman 2014).

The formulation adopted in this article was based on the assumption that the structure undergoes large deformation with small strains. However, if the strains are large or if the material behaviour is nonlinear, different formulations will be required for the nonlinear modelling. The test cases studied in this article (cantilever beam and slender beam) are frequently used benchmark problems within the topology optimization community, allowing the comparison of Iso-XFEM solutions with the solutions from previously developed methods such as SIMP and BESO. Moreover, cantilever and slender beam members exist in many engineering applications, from microscale parts, *e.g.* atomic force microscope cantilevers and micro-electromechanical system cantilevers/beams, to large structures, *e.g.* bridges and civil structures. The application of the method to real problems may require the definition of alternative objective functions and the derivation of appropriate sensitivities. Examples are the design of compliant mechanisms, where the objective can be to maximize the output deformation, and the design of energy absorption structures, where the objective may be to maximize the total absorbed energy.

6. Summary and conclusions

In this study, the topology optimization of geometrically nonlinear structures was investigated, assuming that the structures undergo large displacement with small strain. The Iso-XFEM method was extended to enable the generation of high-resolution topology optimized solutions for geometrically nonlinear structures. A total Lagrangian FE formulation was used to model the geometrically

nonlinear behaviour of continuum structures and a Newton–Raphson iterative method was used to find the equilibrium solution at each load increment. The nonlinear FE code developed for 2D structures was then integrated into the Iso-XFEM method to enable the topology optimization of structures undergoing large deformation. A filter scheme was used in the method to increase the stability of the evolutionary optimization approach applied to nonlinear structures.

The topology optimization results achieved by implementing linear and nonlinear modelling showed that, for the presented test cases, a nonlinear-based optimization returns solutions that are dependent on the magnitude of the load. In addition, the solutions achieved from the optimization using nonlinear modelling have a higher performance than those with linear modelling. Although in the first test case of this study, there is not a significant difference between the solutions achieved from linear and nonlinear modelling, the results from the second test case, which involves snap-through effects, showed the importance of implementing nonlinear modelling in large-displacement problems. As the solutions achieved from the proposed method are represented with clearly defined and smooth boundaries, the time-consuming post-processing stage before manufacturing can be eliminated. This makes the method suitable for the stiffness design of digitally manufactured structures, *e.g.* 3D printed structures, which experience large deformation.

Disclosure statement

No potential conflict of interest was reported by the authors.

Funding

This work was supported by the Engineering and Physical Sciences Research Council [grant number EP/I033335/2].

ORCID

Meisam Abdi http://orcid.org/0000-0003-2320-7509
Ian Ashcroft http://orcid.org/0000-0002-5118-1804
Ricky Wildman http://orcid.org/0000-0003-2329-8471

References

Abdi, M., I. Ashcroft, and R. Wildman. 2014. "An X-FEM Based Approach for Topology Optimization of Continuum Structures." In *Simulation and Modeling Methodologies, Technologies and Applications*, 277–289. Cham: Springer International Publishing.

Abdi, M., I. Ashcroft, and R. Wildman. 2014. "*High Resolution Topology Design with Iso-XFEM*." In *Proceedings of the 25th Solid Freeform Fabrication Symposium (SFF2014)*, 1288–1303. https://sffsymposium.engr.utexas.edu/sites/default/files/2014-101-Abdi.pdf

Abdi, M., R. Wildman, and I. Ashcroft. 2014. "Evolutionary Topology Optimization Using the Extended Finite Element Method and Isolines." *Engineering Optimization* 46 (5): 628–647.

Allaire, G., F. Jouve, and A. M. Toader. 2004. "Structural Optimization Using Sensitivity Analysis and a Level-Set Method." *Journal of Computational Physics* 194 (1): 363–393.

Aremu, A., I. Ashcroft, R. Wildman, R. Hague, C. Tuck, and D. Brackett. 2011. "*A Hybrid Algorithm for Topology Optimization of Additive Manufactured Structures*." In *Proceedings of the 22nd Solid Freeform Fabrication Symposium (SFF2011)*, 279–289. https://sffsymposium.engr.utexas.edu/Manuscripts/2011/2011-22-Aremu.pdf

Aremu, A., I. Ashcroft, R. Wildman, R. Hague, C. Tuck, and D. Brackett. 2013. "The Effects of Bidirectional Evolutionary Structural Optimization Parameters on an Industrial Designed Component for Additive Manufacture." *Proceedings of the Institution of Mechanical Engineers, Part B: Journal of Engineering Manufacture* 227 (6): 794–807.

Bathe, K. J. 2006. *Finite Element Procedures*. Englewood Cliffs, NJ: Prentice Hall.

Bendsøe, M. P. 1989. "Optimal Shape Design as a Material Distribution Problem." *Structural Optimization* 1: 193–202.

Bendsøe, M. P., and N. Kikuchi. 1988. "Generating Optimal Topologies in Structural Design Using a Homogenization Method." *Computer Methods in Applied Mechanics and Engineering* 71: 197–224.

Bruns, T. E., and D. A. Tortorelli. 1998. "Topology Optimization of Geometrically Nonlinear Structures and Compliant Mechanisms." In *Proceedings of the 7th AIAA/USAF/NASA/ISSMO Symposium on Multidisciplinary Analysis and Optimization*, 1874–1882. St. Louis, MO: AIAA.

Bruns, T. E., and D. A. Tortorelli. 2003. "An Element Removal and Reintroduction Strategy for the Topology Optimization of Structures and Compliant Mechanisms." *International Journal for Numerical Methods in Engineering* 57 (10): 1413–1430.
Buhl, T., C. B. Pedersen, and O. Sigmund. 2000. "Stiffness Design of Geometrically Nonlinear Structures Using Topology Optimization." *Structural and Multidisciplinary Optimization* 19 (2): 93–104.
Fiore, A., G. C. Marano, R. Greco, and E. Mastromarino. 2016. "Structural Optimization of Hollow-Section Steel Trusses by Differential Evolution Algorithm." *International Journal of Steel Structures* 16 (2): 411–423.
Gea, H. C., and J. Luo. 2001. "Topology Optimization of Structures with Geometrical Nonlinearities." *Computers & Structures* 79 (20): 1977–1985.
Ha, S. H., and S. Cho. 2008. "Level Set Based Topological Shape Optimization of Geometrically Nonlinear Structures Using Unstructured Mesh." *Computers & Structures* 86 (13): 1447–1455.
He, Q., Z. Kang, and Y. Wang. 2014. "A Topology Optimization Method for Geometrically Nonlinear Structures with Meshless Analysis and Independent Density Field Interpolation." *Computational Mechanics* 54 (3): 629–644.
Huang, X. H., and Y. Xie. 2007. "Bidirectional Evolutionary Topology Optimization for Structures with Geometrical and Material Nonlinearities." *AIAA Journal* 45 (1): 308–313.
Huang, X., and Y. M. Xie. 2008. "Topology Optimization of Nonlinear Structures Under Displacement Loading." *Engineering Structures* 30 (7): 2057–2068.
Huang, X., and M. Xie. 2010. *Evolutionary Topology Optimization of Continuum Structures: Methods and Applications*. Chichester: John Wiley & Sons.
Jakiela, M. J., C. Chapman, J. Duda, A. Adewuya, and K. Saitou. 2000. "Continuum Structural Topology Design with Genetic Algorithms." *Computer Methods in Applied Mechanics and Engineering* 186 (2): 339–356.
Jog, C. 1996. "Distributed-Parameter Optimization and Topology Design for Non-linear Thermoelasticity." *Computer Methods in Applied Mechanics and Engineering* 132 (1–2): 117–134.
Lahuerta, R. D., E. T. Simões, E. M. Campello, P. M. Pimenta, and E. C. Silva. 2013. "Towards the Stabilization of the Low Density Elements in Topology Optimization with Large Deformation." *Computational Mechanics* 52 (4): 779–797.
Li, L., M. Y. Wang, and P. Wei. 2012. "XFEM Schemes for Level Set Based Structural Optimization." *Frontiers of Mechanical Engineering* 7 (4): 335–356.
Luo, Z., and L. Tong. 2008. "A Level Set Method for Shape and Topology Optimization of Large-Displacement Compliant Mechanisms." *International Journal for Numerical Methods in Engineering* 76 (6): 862–892.
Nana, A., J. C. Cuillière, and V. Francois. 2016. "Towards Adaptive Topology Optimization." *Advances in Engineering Software* 100: 290–307.
Panesar, A., D. Brackett, I. Ashcroft, R. Wildman, and R. Hague. 2017. "Hierarchical Remeshing Strategies with Mesh Mapping for Topology Optimisation." *International Journal for Numerical Methods in Engineering* 111: 676–700. doi:10.1002/nme.5488.
Pedersen, C. B., T. Buhl, and O. Sigmund. 2001. "Topology Synthesis of Large-Displacement Compliant Mechanisms." *International Journal for Numerical Methods in Engineering* 50 (12): 2683–2705.
Querin, O. M., G. P. Steven, and Y. M. Xie. 1998. "Evolutionary Structural Optimisation (ESO) Using a Bidirectional Algorithm." *Engineering Computations* 15 (8): 1031–1048.
Sigmund, O. 2001. "A 99 Line Topology Optimization Code Written in Matlab." *Structural and Multidisciplinary Optimization* 21 (2): 120–127.
Sukumar, N., D. L. Chopp, N. Moës, and T. Belytschko. 2001. "Modeling Holes and Inclusions by Level Sets in the Extended Finite-Element Method." *Computer Methods in Applied Mechanics and Engineering* 190 (46): 6183–6200.
van Dijk, N. P., M. Langelaar, and F. van Keulen. 2014. "Element Deformation Scaling for Robust Geometrically Nonlinear Analyses in Topology Optimization." *Structural and Multidisciplinary Optimization* 50 (4): 537–560.
Victoria, M., P. Martí, and O. M. Querin. 2009. "Topology Design of Two-Dimensional Continuum Structures Using Isolines." *Computers & Structures* 87 (1): 101–109.
Victoria, M., O. M. Querin, and P. Martí. 2010. "Topology Design for Multiple Loading Conditions of Continuum Structures Using Isolines and Isosurfaces." *Finite Elements in Analysis and Design* 46 (3): 229–237.
Wang, Y., Z. Kang, and Q. He. 2013. "An Adaptive Refinement Approach for Topology Optimization Based on Separated Density Field Description." *Computers & Structures* 117: 10–22.
Wang, Y., Z. Kang, and Q. He. 2014. "Adaptive Topology Optimization with Independent Error Control for Separated Displacement and Density Fields." *Computers & Structures* 135: 50–61.
Wang, F., B. S. Lazarov, O. Sigmund, and J. S. Jensen. 2014. "Interpolation Scheme for Fictitious Domain Techniques and Topology Optimization of Finite Strain Elastic Problems." *Computer Methods in Applied Mechanics and Engineering* 276: 453–472.
Wang, M. Y., X. Wang, and D. Guo. 2003. "A Level Set Method for Structural Topology Optimization." *Computer Methods in Applied Mechanics and Engineering* 192 (1): 227–246.
Xie, Y. M., and G. P. Steven. 1993. "A Simple Evolutionary Procedure for Structural Optimization." *Computers & Structures* 49: 885–896.
Xie, Y. M., and G. P. Steven. 1997. *Evolutionary Structural Optimization*. London: Springer-Verlag.

Yamasaki, S., S. Yamanaka, and K. Fujita. 2017. "Three-Dimensional Grayscale-Free Topology Optimization Using a Level-Set Based r-Refinement Method." *International Journal for Numerical Methods in Engineering* 112: 1402–1438. doi:10.1002/nme.5562.

Yang, X. Y., Y. M. Xie, G. P. Steven, and O. M. Querin. 1999. "Bidirectional Evolutionary Method for Stiffness Optimization." *AIAA Journal* 37 (11): 1483–1488.

Zhou, M., and G. I. N. Rozvany. 1991. "The COC Algorithm, Part II: Topological, Geometrical and Generalized Shape Optimization." *Computer Methods in Applied Mechanics and Engineering* 89: 309–336.